

Spray Fabrication of Additive-Free Electrodes for Advanced Lithium-Ion Storage Technologies

Sang Ho Lee^{1,*} and Patrick S. Grant²

¹ Department of Chemical Engineering, Pukyong National University, Busan
48513, South Korea.

²Department of Materials, University of Oxford, Oxford OX1 3PH, UK.

* Address correspondence to sangho.lee@pknu.ac.kr

Abstract

Polymer binders and carbon conductivity enhancers are inevitably required to make improvements in structural durability and electrochemical performance of lithium-ion battery (LIB) electrodes, although these additive constituents incur weight and volume penalties on the overall battery capacity. Here, additive-free electrode architectures were successfully fabricated over $20 \times 20 \text{ cm}^2$ electrode areas using a layer-by-layer spray coating approach, with the ultimate goal to boost gravimetric/volumetric electrode capacity and to reduce the total cost of LIB cells. Initially, a binder fraction of spray-coated $\text{Li}_4\text{Ti}_5\text{O}_{12}$ (LTO) electrodes was reduced progressively, from 40 to 0 wt%. The electrochemical behavior of electrodes was then re-optimized as a proportion of conductivity enhancers within the binder-free electrode decreased to “zero”. Further, the otherwise identical spray coating process was applied to manufacture LiFePO_4 (LFP) positive electrodes, leading to all-additive-free full-cell LIB configurations with attractive energy density of $\sim 310 \text{ Wh/kg}$ and power performance of $\sim 1500 \text{ W/kg}$.

Keywords

Spray coating, polymeric binder, conductivity enhancer, $\text{Li}_4\text{Ti}_5\text{O}_{12}$, LiFePO_4 , lithium-ion battery.

1. Introduction

A film-type electrode structure, a dominant format for both negative and positive electrodes, has contributed greatly to reducing the overall weight and volume of LIB cells while providing sufficient energy storage density (~ 250 Wh/kg or ~ 650 Wh/L) and high cell voltage (~ 3.7 V).^[1-5] Moreover, thin film electrodes led to remarkable breakthroughs in a freedom of LIB designs, e.g. from multi-stacked pouch-type cells to the next generation of flexible electrode configurations.^[6-9] In line with continuing demands for thinner and lighter wireless power supplies for use in smart electronics including smartphones, smartwatches and tablet computers, LIBs have come to become the most preferred device in the global energy storage market.^[10-12]

In the manufacture of LIB electrodes, slurry casting is currently the most effective and productive method, where a composite slurry comprising active materials, carbon conductivity enhancers and polymeric binders is coated onto the current collector using a doctor blade coater and then thoroughly dried in order to form an electrode film structure.^[13-17] The structural integrity and performance of the resulting slurry-cast electrode tend to be affected significantly by electrochemically inactive additives such as binders and conductivity enhancers. For example, binder materials often fill and block inter-connected porosities formed between electrode particulates, hindering effective mass transfer of active ions throughout overall electrode structures.^[18,19] By contrast, a lack of binder fractions may decrease physical cohesion between the inter-connected particulates within the resulting electrode and/or between the current collector and electrode layers, resulting in catastrophic capacity degradation at fast charging rates and over repeated charge/discharge cycles.^[20,21] An increase in a fraction of

conductive carbons within electrodes is helpful for improving electrode rate capability but inversely causes a decline in both gravimetric and volumetric electrode capacities because they contribute only to parasitic weights and volumes in the actual electrode capacity estimation.^[22-24] In light of this perspective, there are growing demands to explore alternative manufacturing approaches that ensure the manufacture of mechanically durable and electrochemically superior electrode structures, even when employing a limited quantity of conductive carbons and binders.

A spray coating is one of the film manufacturing techniques,^[25-28] in which solid constituents are suspended into fugitive solvent carriers and then sprayed onto the desired surface. The spray coating enables a wide range of film configurations to be reliably reproduced in large areas of various substrates regardless of their surface wettability and roughness. In contrast to slurry casting, where a thick layer of the bulk slurry is applied onto the current collector all at once, the spray coating process involves multiple passes, with each pass depositing a thin sub-layer of electrode constituents, layer-by-layer, allowing for the gradual development of electrode layers by repeating, reciprocating spray scans. In this respect, the layer-by-layer spray deposition mechanism may show promise in fabricating LIB electrodes even with few additives.

In this research, the potential of fabricating additive-free LIB electrodes was explored using the layer-by-layer spray coating approach. Initially, a portion of polymer binders decreased within spray-coated LTO negative electrodes systematically, from 40 to 0 wt%. Conductive carbon fractions within the binder-free electrode were then reduced again to 0 wt% in order to achieve additive-free electrode structures. The spray-coated additive-free electrode comprising LTO

only had marked improvements in both gravimetric/volumetric capacities and high-rate performance, with a capacity of ~ 175 mAh/g at 0.1 C (almost same as the theoretical capacity of LTO) and ~ 70 % of the state of charge at 20 C. The arising insight was applied equally to LFP positive electrodes, aiming to complete an additive-free LIB configuration in full. The resulting additive-free LIB arrangement, formulated with a 1:1 LTO:LFP capacity ratio, had a stable, comparable specific energy density of ~ 310 Wh/kg and a marked power density of 1500 W/kg. Furthermore, the double-sided electrode fabrication over $\sim 20 \times 20$ cm² electrode areas highlights the immense potential of the spray coating approach for its applicability to grid-scale energy storage systems.

2. Experimental section

Materials: LTO and carboxymethyl cellulose (CMC) binder were obtained from Sigma Aldrich, UK; Super P (SP) conductivity enhancer from MTI Corporation, USA; and LFP from Hydro-Québec, Canada.

Spray coating process: To prepare the spray suspension, active materials (LTO or LFP), SP and CMC in controlled weight fractions were homogeneously blended into a 70:30 mixture (by volume) of de-ionized (DI) water ($\leq 5 \mu\text{S}/\text{cm}$) and isopropyl alcohol (IPA, 99.5 %) using ultrasonication. The prepared suspension was pumped and subsequently atomized at the spray nozzle using a compressed air pressure of 0.4 bar. The nozzle was reciprocated back and forth in a pre-programmed path, such as a zig-zag pattern in the x and y plane with a fixed spray distance z . No calendaring was conducted for all spray-coated electrodes.

Electrochemical testing: The electrochemical behavior of the arising spray-coated electrodes was investigated using coin-type battery cells (CR2032) that were assembled in an Ar-filled glovebox ($\text{H}_2\text{O} < 0.1 \text{ ppm}$, $\text{O}_2 < 0.1 \text{ ppm}$). Prior to the cell assembly, coin cell components including spray-coated electrodes were thoroughly dried in the oven overnight. For half-cells, spray-coated LTO (or LFP) electrodes were coupled with pure lithium foils (99.9 % trace metals basis, MTI, USA) that were used as a counter/reference electrode. Full-cell LIB configurations were prepared by coupling spray-coated LTO negative electrodes with spray-coated LFP positive electrodes. Two electrodes were electrically and physically separated by a polypropylene separator (Celgard 2400, UK) that was fully soaked into 1 M LiPF_6 electrolyte solution in a 1:1 mixture (by volume) of ethylene carbonate and dimethyl carbonate (Sigma Aldrich, UK). Charge/discharge measurements for both half-cell and full-cell configurations were carried out at

room temperature using Arbin BT2000 cyclers. The electrochemical performances of full-cell LIBs were estimated based on the total weight of the LTO negative electrode including LTO, SP and CMC. Electrochemical impedance spectroscopy (EIS) was examined after the first three cyclic voltammetry (CV) cycles using Gamry 600 potentiostats. The theoretical capacity of both LTO and LFP materials was assumed to be $\sim 175 \text{ mAh/g}$.^[29-32]

3. Results and discussion

The initial exploration of additive-free LIB electrode fabrication involved a stepwise reduction in the proportion of CMC binders within spray-coated LTO-based electrodes, starting from 40 to 0 wt%, as summarized in comparative bar graphs in Figure 1a. Here, a portion of SP conductivity enhancers was maintained constantly at ~10 wt% for all cases. As CMC fractions within electrodes decreased to 0 wt%, LTO fractions increased correspondingly from 50 to 90 wt%. Figures 1b-f exhibit a series of scanning electron microscope (SEM) images for the surface of the resulting spray-coated LTO electrodes with varying CMC fractions. The excessive use of CMC in the electrode fabrication process (e.g. 40 wt% and 20 wt% CMC) were shown to facilitate the filling of void spaces that arise between electrode particles, as shown in Figures 1b and 1c. However, as CMC fractions were reduced to 10 wt% or less, it was evident that beneficial inter-connected porosities within the spray-coated electrode were clearly visible and not fully blocked by CMC molecules (Figures 1d-f). The corresponding electrode cross-sections in the left-hand insets of each figure show that the electrode thickness remained consistent at approximately 20 μm for all cases (also, see Table 1). Here, a relatively thin electrode layer was prioritized to investigate the feasibility of manufacturing additive-free electrode configurations over large current collector areas.

The electrochemical behavior of the identical spray-coated LTO electrodes was then studied at increasing charge/discharge rates of 0.1, 0.2, 0.5, 1, 2, 5, 10 and 20 C, as shown in Figure 2a. As the CMC fraction decreased from 40 to 0 wt% (inversely the LTO portion increased from 50 to 90 wt%), gravimetric discharge capacities of the spray-coated LTO electrodes increased markedly at all rates.

Note that the electrode capacity was estimated based on the total electrode mass including LTO, SP and CMC, providing a more realistic and comprehensive representation of the overall electrode capacity. At 20 C, the binder-free electrode, formulated with a LTO:SP:CMC mass ratio of 90:10:0, delivered the highest discharge capacity of ~ 110 mAh/g, whereas a capacity of the electrode with 40 wt% CMC dropped below 10 mAh/g (see Table 1). Additionally, the electrode capacities were estimated using the LTO weight only (Figure S1 in the Supporting Information), aiming to investigate the inherent impact of CMC binder fractions on the electrochemical behavior of electrodes. At 20 C, the spray-coated binder-free electrode still had the highest capacity of ~ 130 mAh/g, while an excessive amount of binders (i.e. 40 wt% CMC) was shown to be still unhelpful for delivering the intrinsic electrode capacity. Further, the approach of minimizing binder fractions within the spray-coated electrode had a significant benefit in volumetric performance, as shown in Figure S2 of the Supporting Information. Here, volumetric capacities were re-estimated by normalizing the gravimetric data (Figure 2a) by the electrode mass and thickness (Table 1). Consistent with the gravimetric capacity tendency, the spray-coated binder-free LTO electrode (90:10:0 formulation) had superior performances per unit volume over other electrodes with 5, 10, 20 and 40 wt% CMC. Particularly, at 20 C the volumetric capacity of the binder-free electrode (~ 150 mAh/cm³) was an order of magnitude greater than that of the electrode with 40 wt% CMC (~ 14 mAh/g).

The electrochemical behavior as a function of CMC fractions was further studied using EIS measurements, as shown in Figure 2b. In the Nyquist plots for the identical spray-coated LTO electrodes (the inset magnifies the Nyquist curves for the electrodes with 0, 5 and 10 wt% CMC), the size of the semi-circle

decreased markedly as the CMC fraction decreased from 40 to 0 wt%, indicating the reduction in the charge transfer resistance of the electrode through decreasing the insulating binder proportion. As a result, the binder-free electrode had the smallest electrode impedance ($\sim 63 \Omega$), which made a marked contribution to electrode rate capability especially at 20 C.

The galvanostatic discharge capacity profiles at a constant charge/discharge rate of 1 C support the structural integrity of the spray-coated electrode, as shown in Figure 2c. After 300 cycles, the binder-free electrode retained the highest discharge capacity of ~ 140 mAh/g, which corresponds to ~ 97 % capacity retention (compared with the 1st discharge capacity value). At the 300th cycle, spray-coated LTO electrodes with 5 and 10 wt% CMC delivered discharge capacities of ~ 130 mAh/g and ~ 110 mAh/g, respectively, while electrodes with 20 and 40 wt% CMC had capacities dropped to ~ 60 mAh/g and ~ 10 mAh/g, respectively. All the electrodes sustained almost 100 % coulombic efficiency after 300 cycles, as shown in the inset.

The impact of the binder-free electrode on the charge/discharge reaction kinetics was explored through investigating the lithium-ion diffusion coefficient. Here, the ion diffusion coefficient was estimated from CV measurements at increasing scan rates of 0.1, 0.2, 0.5, 1.0, 2.0 and 5.0 mV/s, as shown in Figure S3 of the Supporting Information. As the scan rate increased from 0.1 to 5.0 mV/s, the anodic current density peaks at ~ 1.75 V increased for all electrode cases, characteristics of spinel LTO.^[33,34] However, the extent of the peak current density increment was shown to depend on CMC proportions within the electrode. For instance, as the CMC fraction decreased from 40 to 0 wt%, the peak intensity increased markedly with increasing scan rates, indicating a difference in ion

mobility according to electrode structures and compositions. Figure 3a represents plots of the anodic peak current density against the square root of the scan rate as a function of CMC fractions, showing that the peak current density was a best linear-fit relation to the square root of the scan rate. Thus, the lithium-ion diffusion coefficient could be estimated using the Randles-Sevcik equation.^[35,36]

$$I_p = 0.4463n F A C_0 (n F v D_{Li} / RT)^{1/2} \quad (1)$$

where I_p was the peak current [A], n was the number of electrons transferred, F was the Faraday constant [C/mol], A was the electrode area [cm²], C_0 was the molar concentration of the lithium-ions in the electrode [mol/cm³], D_{Li} was the lithium-ion diffusion coefficient [cm²/s], v was the scan rate [V/s], R was the Gas constant [J/K·mol], and T was the temperature [K]. The comparative bar graphs in Figure 3b show effective ion diffusion coefficient estimates for the spray-coated LTO electrodes as a function of the CMC binder. As CMC fractions decreased to 0 wt%, the diffusion coefficient of the spray-coated LTO electrodes increased markedly. Consequently, the binder-free electrode (90:10:0 formulation) had the highest diffusion coefficient value of $\sim 4 \times 10^{-12}$ cm²/s (see Table 1), supporting a hypothesis that binder minimization in electrode could boost accessibility of active ions throughout the entire electrode structure.

Figure 4 presents a schematic illustration of how the spray coating process can construct electrode layers over large current collector areas. To accomplish the successful layer-by-layer spray coating, the spray suspension should have sufficiently rheological properties without any sedimentation of the solid constituents, ensuring stable pumping of the suspension to the spray nozzle and

continuous atomization into droplets at the nozzle tip. For the suspension preparation, the bi-solvent carrier of DI water and IPA was utilized, where DI water was required to dissolve water-soluble CMC while IPA helped to disperse carbon-based SP effectively into the predominantly aqueous solution. The current collector was fixed on a vacuum chuck of a hot plate that was then heated to a pre-set temperature ($> 100\text{ }^{\circ}\text{C}$). It is critical that the heated current collector enables the fast, effective drying of a suspension layer deposited during the electrode fabrication process before the next layer is applied, leading to the successive superimposition of sub-layers over the pre-formed layer, layer-by-layer. Moreover, this allows for precise control over the layer thickness and prevents excessive build-up or uneven distribution of the electrode material. A photograph in Figure 4 shows the mechanically durable behavior of the as-fabricated binder-free electrode on a Cu foil. The spray-coated binder-free electrode maintained its physical integrity without any significant signs of damage or detachment from the current collector even after flexing and bending vigorously. Overall, the layer-by-layer assembly approach was likely to give rise to a closely packed arrangement of electrode constituents within the resulting binder-free electrode matrix, allowing for effective interaction between the inter-connected particulates even with reduced binder fractions, as depicted in the magnified cartoon in Figure 4. Also, Figure S4 in the Supporting Information depicts the binder-free electrode fabrication through spray coating.

To realize the full potential of the layer-by-layer spray coating on practical lithium-ion storage technologies, a possibility of reducing the fraction of SP conductivity enhancers within the binder-free electrode was further explored. The thermogravimetric analysis (TGA) curves in Figure S5 of the Supporting

Information verify a progressive decrease in the SP fraction within the binder-free LTO electrodes, from 10 to 0 wt%. Figure 5a shows electrode discharge capacities at increasing rates of 0.1 to 20 C as a function of the SP proportion, noting that the electrode capacity was estimated on the basis of the total electrode mass including LTO and SP. The spray-coated additive-free LTO electrode comprising LTO only (100:0:0 formulation) had superior rate capability over other binder-free electrodes formulated with 5 and 10 wt% SP, with discharge capacities of ~ 175 mAh/g at 0.1 C and ~ 120 mAh/g at 20 C (see Table 2). The inset of Figure 5a presents the rate capacity retention as a function of the SP fraction within the binder-free LTO electrode, where the capacity retention is defined as the ratio of the discharge capacity values obtained at 0.1, 0.2, 0.5, 1.0, 2.0, 5.0, 10.0 and 20.0 C to the discharge capacity at 0.1 C. At 20 C, the additive-free LTO electrode retained ~ 70 % capacity retention, and other binder-free electrodes with 5 and 10 wt% SP had slightly lower retention values of ~ 67 % and ~ 66 %, respectively.

The electrochemical charge/discharge mechanism of the spray-coated additive-free electrode was examined at increasing charge/discharge rates. In Figure 5b, it was observed that there were voltage plateaus at around 1.5 V, which were associated with the de-lithiation characteristics of LTO. Comparative bar graphs in the inset summarized the state of charge (SOC) as a function of SP fractions within the binder-free electrode. Here, SOC is defined as the ratio of the obtained electrode capacity at a certain charging rate to the theoretical capacity of LTO (~ 175 mAh/g). The additive-free LTO electrode (100:0:0 formulation) had ~ 100 % full lithiation at 0.1 C and ~ 70 % SOC at 20 C, signifying its superior ability to effectively store and release lithium ions. In Figure 5c, galvanostatic discharge capacity profiles at a constant charge/discharge rate of 1 C support the

stable cycle life of the spray-coated additive-free LTO electrode. After 500 cycles, the additive-free electrode sustained a discharge capacity of ~ 150 mAh/g, whereas the electrodes with 5 and 10 wt% SP had a discharge capacity of ~ 140 mAh/g and ~ 120 mAh/g, respectively. Regardless of SP fractions, the spray-coated binder-free electrodes had outstanding capacity retention of $> 90\%$, only with slightly higher retention of $\sim 95\%$ for the additive-free LTO electrode (left-hand inset). All the electrodes had $\sim 100\%$ coulombic efficiency up to the 500th cycle, as shown in Figure S6 of the Supporting Information. The right-hand photograph in Figure 5c represents the binder-free LTO electrode with 0, 5 and 10 wt% SP (from left to right). As the SP fraction was reduced gradually from 10 to 0 wt% (the LTO fraction increased inversely to 100 wt%), the electrode became noticeably whiter, noting that a white LTO powder was used in the electrode fabrication. This change in color shows the increasing dominance of LTO as the SP proportion within the binder-free electrode decreased progressively.

The arising insight of minimizing electrochemically inactive additives in the electrode was applied equally to a spray-coated LFP positive electrode, which intended to complete an additive-free full-cell configuration. Figures S7a and S7b in the Supporting Information show gravimetric and volumetric performance as a function of SP fractions within binder-free LFP electrodes, ranging from 10 to 0 wt%. Consistent with the tendency of the spray-coated LTO electrode, additive-free LFP electrodes exhibited superior energy storage capabilities, both in terms of per unit mass and per unit volume (refer to Table S1 in the Supporting Information). In Figure S7c, the additive-free LFP electrode, cycled at a constant charge/discharge rate of 1 C, sustained a discharge capacity of ~ 130 mAh/g after 300 cycles.

Using the spray-coated LTO and LFP electrodes, performance of full-cell LIB configurations was then investigated, where electrochemical behaviors of spray-coated additive-free LTO/LFP arrangements (denoted as 100:0:0 LIB hereafter) were compared with those of spray-coated LTO/LPF equivalents formulated with a LTO (or LFP):SP:CMC mass ratio of 80:10:10 (denoted as 80:10:10 LIB). Here, an anode-to-cathode capacity ratio was fixed at 1:1 for all cases (please see Table 3). Figure 6a presents gravimetric charge/discharge profiles at 0.1, 1 and 10 C for the 100:0:0 and 80:10:10 LIBs, showing that the 100:0:0 LIB outperformed the 80:10:10 equivalent in terms of deliverable charge/discharge capacities at all rates, especially with charge/discharge capacities of ~ 165 mAh/g at 0.1 C, ~ 140 mAh/g at 1 C and ~ 100 mAh/g at 10 C for the 100:0:0 LIB. Figure 6b shows the Ragone plots at various charge/discharge rates of 0.1, 0.2, 0.5, 1, 2, 5 and 10 C for the 100:0:0 and 80:10:10 LIBs. The 100:0:0 LIB had a specific energy density of ~ 310 Wh/kg at 0.1 C and a specific power density of ~ 1500 W/kg at 10 C, both of which were also superior over those of the 80:10:10 equivalent. The inset photograph presents the double-sided coating of additive-free LTO electrodes on a 20×20 cm² Cu foil, suggesting the potential for efficient and bespoke production of multiple battery stacks for use in pure/hybrid electric vehicles. Figure 6c shows the galvanostatic discharge energy density as a function of charge/discharge cycles at a constant charge/discharge rate of 1 C. After 500 cycles, the 100:0:0 and 80:10:10 LIBs sustained energy densities of ~ 230 Wh/kg and ~ 150 Wh/kg, respectively. Excluding the first few cycles, both the LIBs had almost 100 % coulombic efficiency up to the 500th cycle, as shown the inset.

4. Conclusions

All-additive-free LIB electrodes were successfully developed over large electrode areas of $\geq 20 \times 20 \text{ cm}^2$ using a layer-by-layer spray coating method. The fabrication approach began with decreasing a proportion of CMC binders within the electrode progressively to 0 wt%, and subsequently reducing a fraction of SP conductivity enhancers again to zero in both LTO anodes and LFP cathodes. In half-cell tests, the arising additive-free 100:0:0 LTO electrode had $\sim 70 \%$ SOC and a discharge capacity of $\sim 120 \text{ mAh/g}$ at 20 C, almost double those of 80:10:10 electrode equivalents (e.g. $\sim 37 \%$ SOC and $\sim 66 \text{ mAh/g}$ at 20 C). Particularly, the additive-free LTO/LFP LIB configuration delivered an attractive energy density of $\sim 310 \text{ Wh/kg}$ and power performance of 1500 W/kg , which were found to be either superior or comparable to the electrochemical behaviors of other LTO/LFP LIBs that were prepared by a conventional slurry casting process using higher fractions of parasitic additives (see Table S2 in the Supporting Information).^[37-41] Overall, the layer-by-layer spray coating technique provides a fresh insight into the manufacture of commercial battery electrodes, aiming at maximizing capacity and power capability while minimizing the reliance on performance enhancers or costly and complicated additives. Spray coating may offer an essential and cutting-edge protocol that could negotiate inevitable trade-offs between high energy storage capacity and rapid power response in commercial LIBs through carefully controlling the layering and composition of electrodes.

Acknowledgments

This work was supported by the UK Faraday Institution through grant NEXTRODE - Next generation electrodes number (FIRG015), the National Research Foundation of Korea grant (NRF-2021R1C1C2013340) and the Technology Innovation Program (20019249) funded By the Ministry of Trade, Industry & Energy (MOTIE, Korea). The authors would like to thank Hydro-Québec for providing the LiFePO₄ materials.

References

1. S. H. Lee, C. Huang, P. S. Grant, *Energy Storage Mater.* 38 (2021) 70-79.
2. U. -H. Kim, S. -B. Lee, N. -Y. Park, S. J. Kim, C. S. Yoon, Y. -K. Sun, *ACS Energy Lett.* 7 (2022) 3880-3888.
3. S. H. Lee, *Batteries & Supercaps* 6 (2023) e202200380.
4. M. Kim, S. K. Kang, J. Choi, H. Ahn, J. Ji, S. H. Lee, W. B. Kim, *Nano Lett.* 22 (2022) 10232-10239.
5. X. Zhou, L. Yu, X. -Y. Yu, X. W. Lou, *Adv. Energy Mater.* 6 (2016) 1601177.
6. C. Wang, J. T. Kim, C. Wang, X. Sun, *Adv. Mater.* 35 (2023) 2209074.
7. C. Zhao, Y. Pan, R. Li, A. Hu, B. Zhou, M. He, J. Chen, Z. Yan, Y. Fan, N. Chen, M. Liu, J. Long, *Chem. Eng. J.* 463 (2023) 142386.
8. S. Mukherjee, A. Albertengo, T. Djenizian, *Energy Storage Mater.* 42 (2021) 773-785.
9. Z. Fang, J. Wang, H. Wu, Q. Li, S. Fan, J. Wang, *J. Power Sources* 454 (2020) 227932.

10. S. K. Kang, M. Kim, H. H. Shin, W. Yoon, S. Lee, D. Jang, J. Choi, G. H. Park, J. Park, W. B. Kim, *Adv. Funct. Mater.* 33 (2023) 2300143.
11. Y. Huang, Y. Fang, X. F. Lu, D. Luan, X. W. D. Lou, *Angew. Chem. Int. Ed.* 59 (2020) 19914-19918.
12. S. H. Lee, C. Huang, P. S. Grant, *Nano Energy* 61 (2019) 96-103.
13. C. J. Zhang, W. Zhao, S. -H. Park, T. Guo, S. Deng, A. Seral-Ascaso, M. Si, R. Grissa, S. Barwich, V. Nicolosi, *Adv. Funct. Mater.* 33 (2023) 2213860.
14. T. Liu, L. Zhang, J. Li, Y. Li, K. Lai, S. Zhang, G. Zhao, D. Liu, Z. Xi, C. Liu, L. Ci, *J. Electroanal. Chem.* 928 (2023) 117032.
15. S. H. Lee, C. Huang, C. Johnston, P. S. Grant, *Electrochim. Acta* 292 (2018) 546-557.
16. Y. Ouyang, W. Zong, X. Zhu, L. Mo, G. Chao, W. Fan, F. Lai, Y. -E Miao, T. Liu, Y. Yu, *Adv. Sci.* 9 (2022) 2203181.
17. Y. Li, J. Huang, L. Kang, Z. Tian, F. Lai, D. J. L. Brett, T. Liu, G. He, *Sci. China Mater.* 65 (2022) 1495-1502.
18. F. Hippauf, B. Schumm, S. Doerfler, H. Althues, S. Fujiki, T. Shiratsuchi, T. Tsujimura, Y. Aihara, S. Kaskel, *Energy Storage Mater.* 21 (2019) 390-398.
19. S. H. Lee, A. Mahadevegowda, C. Huang, J. D. Evans, P. S. Grant, *J. Mater. Chem. A* 6 (2018) 13133-13141.
20. F. Zou, A. Manthiram, *Adv. Energy Mater.* 10 (2020) 2002508.
21. N. Lingappan, L. Kong, M. Pecht, *Renewable Sustainable Energy Rev.* 147 (2021) 111227.
22. J. H. Choi, C. Lee, S. Park, M. Hwang, T. J. Embleton, K. Ko, M. Jo, K. S. Saqib, J. Yun, M. Jo, Y. Son, P. Oh, *Electrochem. Commun.* 146 (2023) 10741.

23. Y. Itou, N. Ogihara, S. Kawauchi, *J. Phys. Chem. C* 124 (2020) 5559-5564.
24. S. Ko, Y. Yamada, L. Lander, A. Yamada, *Carbon* 158 (2020) 766-771.
25. J. D. Evans, Y. Sun, P. S. Grant, *ACS Appl. Mater. Interfaces* 14 (2022) 34538-34551.
26. C. Cheng, R. Drummond, S. R. Duncan, P. S. Grant, *J. Power Sources* 448 (2020) 227376.
27. S. H. Lee, C. Huang, P. S. Grant, *Energy Storage Mater.* 33 (2020) 408-415.
28. S. H. Lee, C. Johnston, P. S. Grant, *ACS Appl. Mater. Interfaces* 11 (2019) 37859-37866.
29. D. M. Cunha, T. A. Hendriks, A. Vasileiadis, C. M. Vos, T. Verhallen, D. P. Singh, M. Wagemaker, M. Huijben, *ACS Appl. Energy Mater.* 2 (2019) 3410-3418.
30. M. Ding, H. Liu, X. Zhao, L. Pang, L. Deng, M. Li, *RSC Adv.* 7 (2017) 43894-43904.
31. D. Saikia, J. R. Deka, C. -J. Chou, C. -H. Lin, Y. -C. Yang, H. -M. Kao, *ACS Appl. Energy Mater.* 2 (2019) 1121-1133.
32. L. -H. Hu, F. -Y. Wu, C. -T. Lin, A. N. Khlobystov, L. -J. Li, *Nat. Commun.* 4 (2013) 1687.
33. A. Lakshmi-Narayana, M. Dhananjaya, C. M. Julien, S. W. Joo, C. V. Ramana, *ACS Appl. Mater. Interfaces* 15 (2023) 20925-20945.
34. S. H. Lee, C. Johnston, P. S. Grant, *Energy. Technol.* 8 (2020) 2000253.
35. Y. J. Kim, S. Y. Ko, S. Kim, K. M. Choi, W. -H. Ryu, *Small* 19 (2023) 2206561.
36. S. H. Lee, K. Li, C. Huang, J. D. Evans, P. S. Grant, *ACS Appl. Mater. Interfaces* 11 (2019) 603-612.

37. P. Wang, G. Zhang, J. Cheng, Y. You, Y. -K. Li, C. Ding, J. -J. Gu, X. -S. Zheng, C. -F. Zhang, F. -F. Cao, *ACS Appl. Mater. Interfaces* 9 (2017) 6138-6143.
38. M. Qin, Y. Li, X. -J. Lv, *Nanomaterials* 7 (2017) 150.
39. C. -C. Yang, H. -C. Hu, S. J. Lin, W. -C. Chien, *J. Power Sources* 258 (2014) 424-433.
40. Y. S. Jung, A. S. Cavanagh, L. Gedvilas, N. E. Widjonarko, I. D. Scott, S. -H. Lee, G. -H. Kim, S. M. George, A. C. Dillon, *Adv. Energy Mater.* 2 (2012) 1022-1027.
41. N. Li, Z. Chen, W. Ren, F. Li, H. -M. Cheng, *PNAS* 109 (2012) 17360-17365.

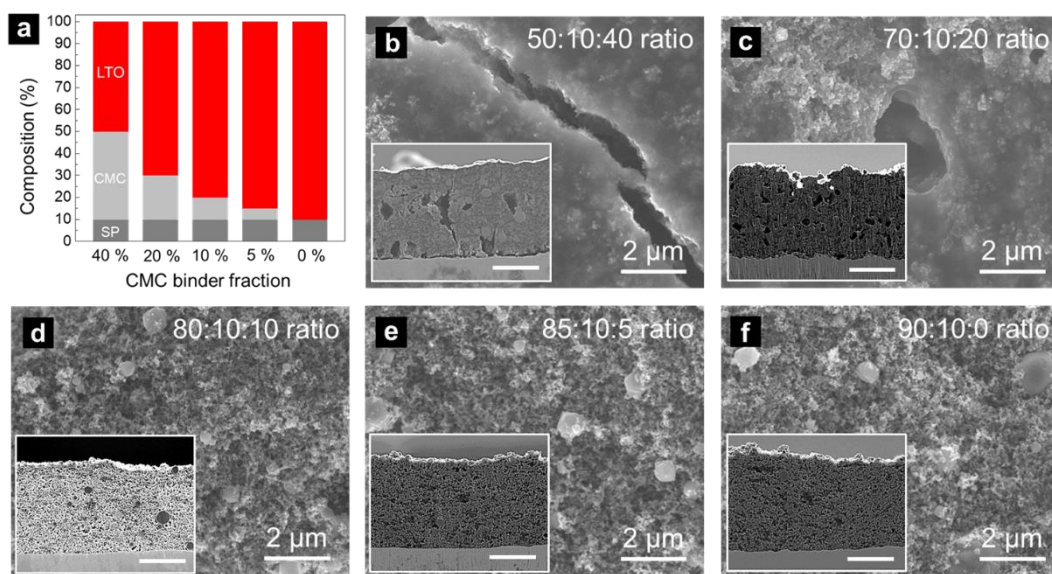


Figure 1. (a) The comparative bar graphs show the change in CMC fractions within the spray-coated LTO electrodes. SEM images for the spray-coated LTO electrodes with varying CMC fractions: (b) 40 wt%, (c) 20 wt%, (d) 10 wt%, (e) 5 wt% and (f) 0 wt%. The left-hand insets represent the cross-section of each electrode. The scale bars in the inset indicate 10 μm .

Table 1. Summary of the spray-coated LTO electrodes as a function of CMC fractions.

Formulation (LTO : SP : CMC)	Thickness (μm)	Mass loading (mg/cm^2)	Discharge capacity (mAh/g)				Diffusion coefficient (cm^2/s)
			0.1 C	1 C	10 C	20 C	
90 : 10 : 0	20 ± 2	3.08 ± 0.02	160	136	120	105	3.92×10^{-12}
85 : 10 : 5	20 ± 2	3.06 ± 0.03	145	130	105	82	3.09×10^{-12}
80 : 10 : 10	20 ± 2	3.02 ± 0.03	130	119	89	66	5.52×10^{-13}
70 : 10 : 20	20 ± 3	2.90 ± 0.02	112	73	35	24	3.28×10^{-13}
50 : 10 : 40	20 ± 3	2.62 ± 0.03	33	15	10	8	2.05×10^{-14}

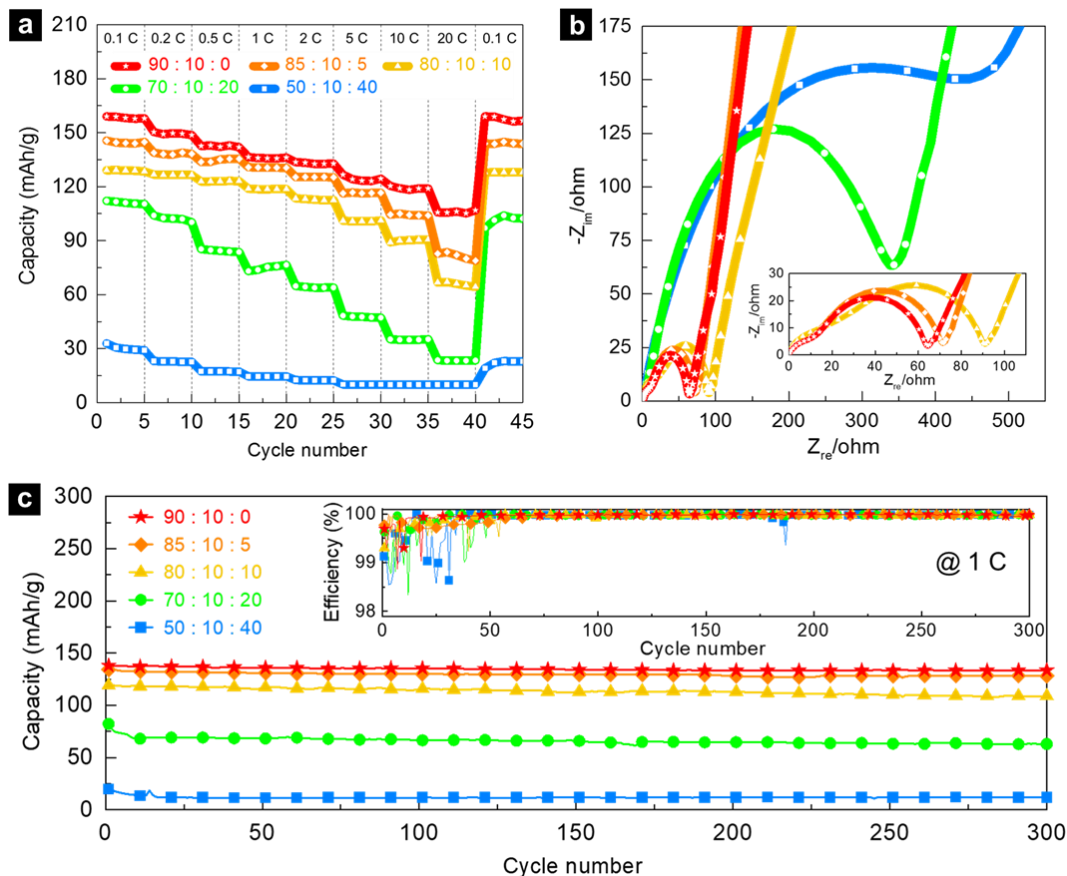


Figure 2. (a) Gravimetric discharge capacity profiles as a function of CMC fractions within the spray-coated LTO electrode at increasing C-rates in the potential range 1.0 to 2.5 V (vs. Li/Li⁺). (b) Corresponding Nyquist plots for the same electrodes. The inset magnifies the Nyquist curves for the electrodes formulated with 0, 5 and 10 wt% CMC. (c) Galvanostatic discharge capacity profiles at a constant charge/discharge rate of 1 C in the potential range 1.0 to 2.5 V (vs. Li/Li⁺). The inset represents the corresponding coulombic efficiency for the same electrodes.

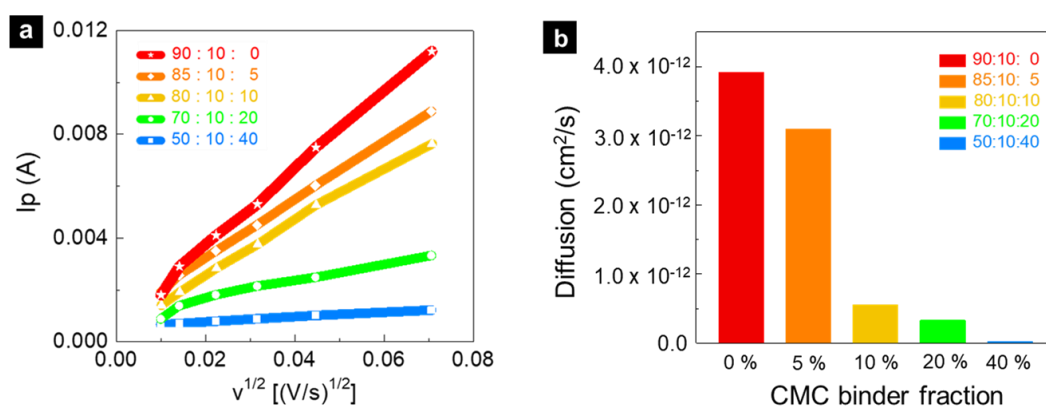


Figure 3. (a) Linear relationships between the anodic current density peaks at approximately 1.75 V and the square root of the scan rate for the spray-coated LTO electrodes with varying CMC fractions. (b) The bar graphs show corresponding lithium-ion diffusion coefficient estimates.

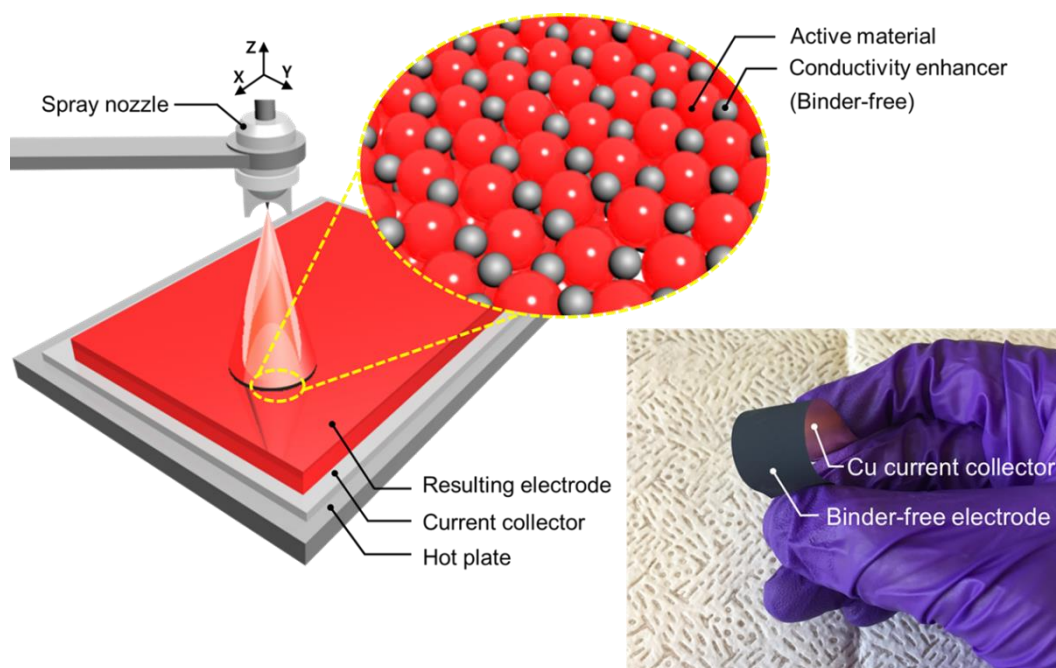


Figure 4. Schematic diagram for spray coating of the binder-free electrode over a large area current collector. The magnified cartoon indicates the idealized arrangement of solid constituents within the binder-free electrode. The right-hand photograph for an as-fabricated binder-free electrode withstanding bending and flexing by hand.

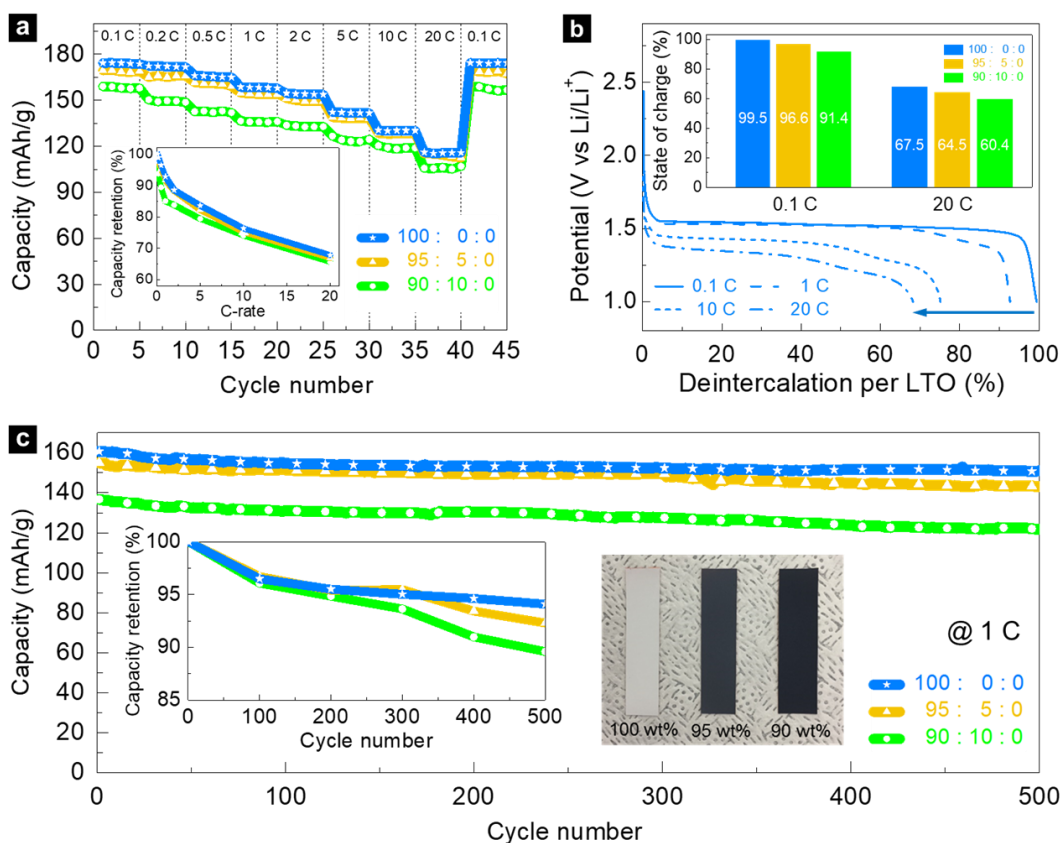


Figure 5. (a) Gravimetric discharge capacity profiles of the spray-coated binder-free LTO electrodes as a function of SP fractions at increasing C-rates in the potential range 1.0 to 2.5 V (vs. Li/Li⁺). The inset shows the corresponding capacity retention as a function of C-rates. (b) The discharge curves of the spray-coated additive-free LTO electrode at 0.1, 1, 10 and 20 C. The comparative bar graphs (inset) show the SOC profiles at 0.1 and 20 C for the binder-free LTO electrodes as a function of SP fractions. (c) Galvanostatic discharge capacity curves of the binder-free electrodes with different SP fractions at 1 C in the potential range 1.0 to 2.5 V (vs. Li/Li⁺). The left-hand inset shows the corresponding capacity retention tendency. The right-hand photograph represents the binder-free electrodes with 0, 5 and 10 wt% SP (from left to right).

Table 2. Summary of the spray-coated binder-free LTO electrodes as a function of SP fractions.

Formulation (LTO : SP : CMC)	Thickness (μm)	Mass loading (mg/cm^2)	Discharge capacity (mAh/g)			
			0.1 C	1 C	10 C	20 C
100 : 0 : 0	20 ± 2	3.16 ± 0.03	174	158	131	116
95 : 5 : 0	20 ± 2	3.12 ± 0.03	169	155	129	113
90 : 10 : 0	20 ± 2	3.08 ± 0.02	160	136	117	97

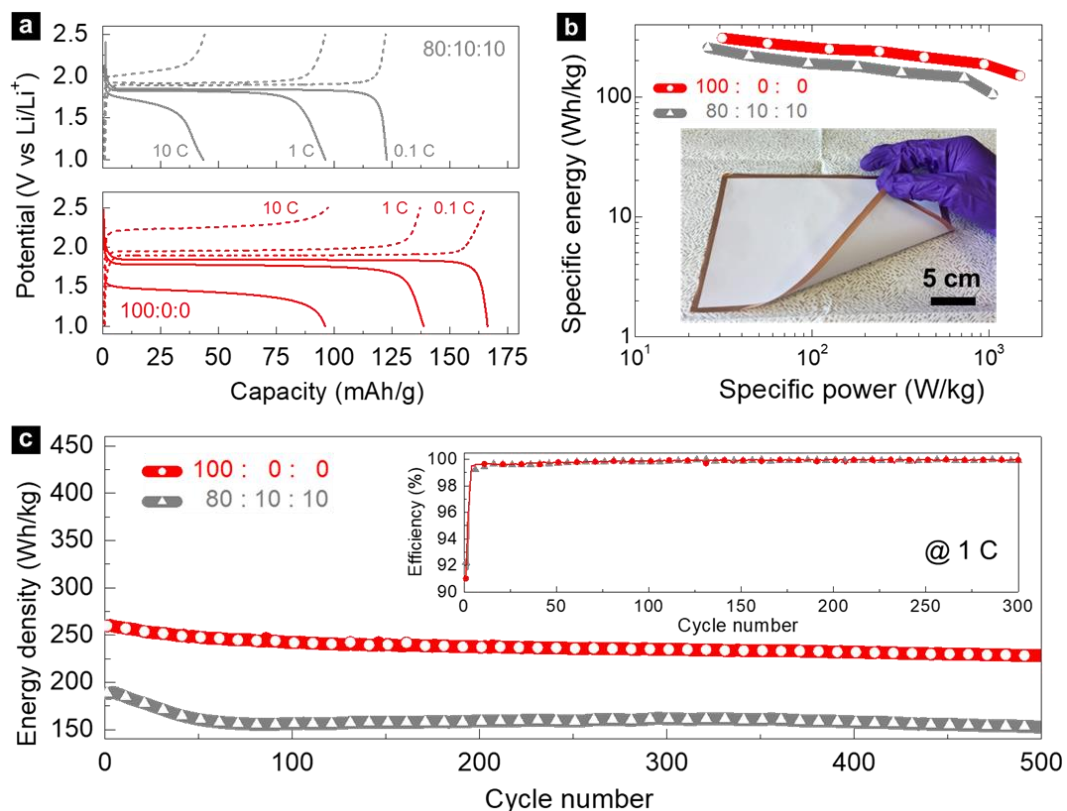


Figure 6. (a) Gravimetric charge/discharge curves at 0.1, 1 and 10 C in the potential range 1.0 to 2.5 V (vs. Li/Li⁺) for the 100:0:0 and 80:10:10 LIBs. (b) Comparative Ragone plots for the 100:0:0 and 80:10:10 LIBs. The inset photograph shows the double-sided fabrication of the additive-free LTO electrode over a 20 × 20 cm² Cu foil. (c) Galvanostatic discharge energy density profiles at 1 C in the potential range 1.0 to 2.5 V (vs. Li/Li⁺). The inset shows the corresponding coulombic efficiency profiles for the identical electrodes.

Table 3. Summary of the 100:0:0 and 80:10:10 LIB configurations.

Formulation (Active : SP : CMC)	Mass loading (mg/cm ²)		Discharge capacity (mAh/g)		
	LTO	LFP	0.1 C	1 C	10 C
100 : 0 : 0	3.16 ± 0.02	3.18 ± 0.02	165	138	95
80 : 10 : 10	3.08 ± 0.03	3.08 ± 0.03	121	96	42

Supporting Information

Spray Fabrication of Additive-Free Electrodes for Advanced Lithium-Ion Storage Technologies

Sang Ho Lee^{1,*} and Patrick S. Grant²

¹Department of Chemical Engineering, Pukyong National University, Busan
48513, South Korea.

²Department of Materials, University of Oxford, Oxford OX1 3PH, UK.

* Address correspondence to sangho.lee@pknu.ac.kr

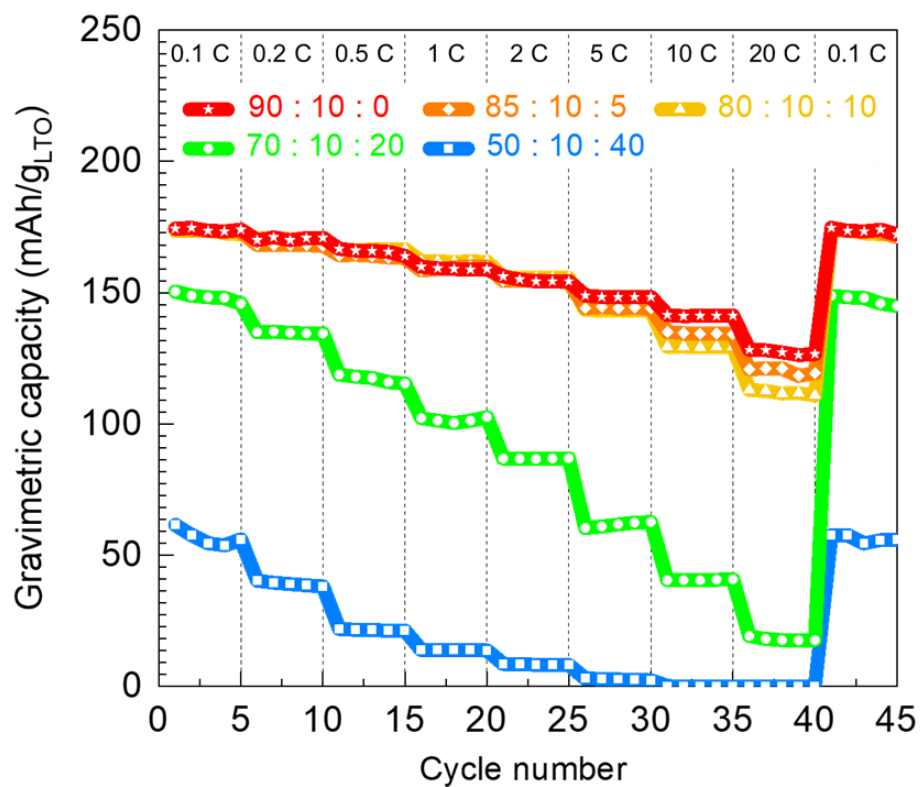


Figure S1. Gravimetric discharge capacity profiles for the spray-coated LTO electrodes with varying CMC fractions at increasing C-rates in the potential range 1.0 to 2.5 V (vs. Li/Li⁺). Here, the electrode capacity was estimated based on the active LTO mass only.

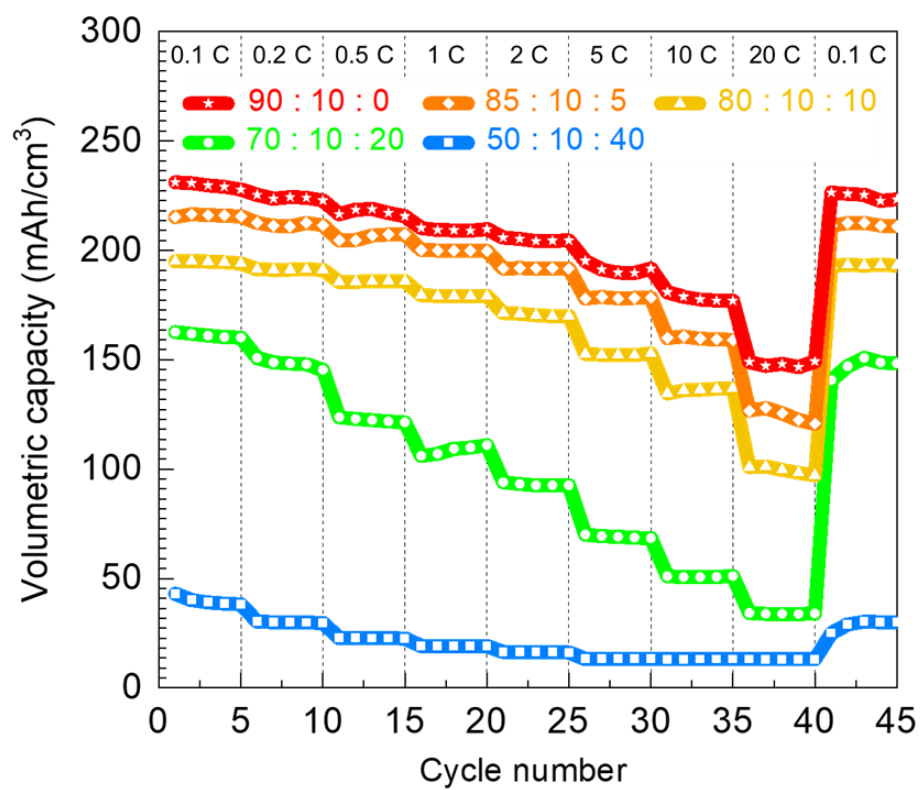


Figure S2. Volumetric discharge capacity plots as a function of CMC fractions within the spray-coated LTO electrode at increasing C-rates in the potential range 1.0 to 2.5 V (vs. Li/Li⁺).

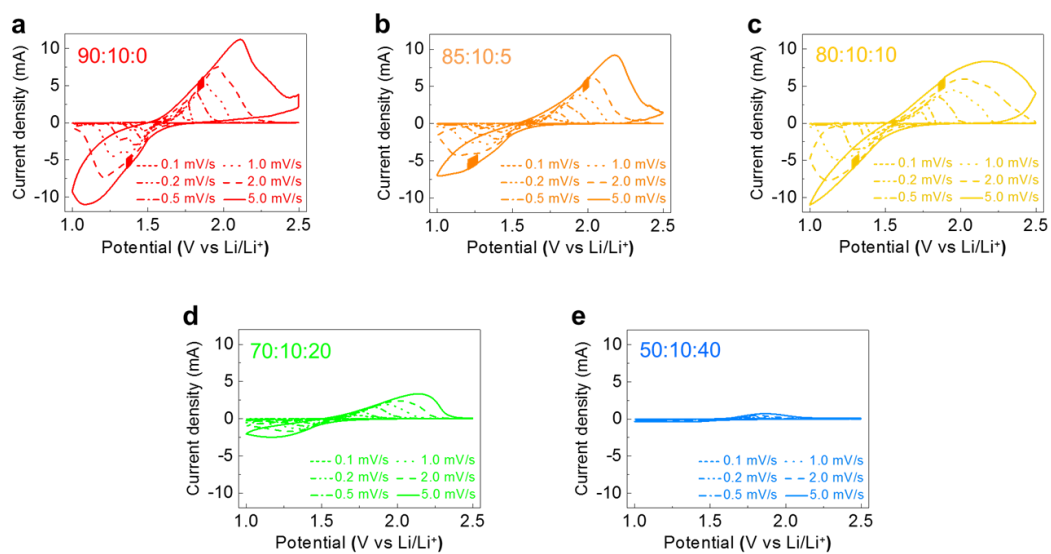


Figure S3. CV curves at various scan rates of 0.1 to 5.0 mV/s in the potential range 1.0 to 2.5 V (vs. Li/Li^+) for the spray-coated LTO electrodes with differing CMC fractions of (a) 0 wt%, (b) 5 wt%, (c) 10 wt%, (d) 20 wt% and (e) 40 wt%.

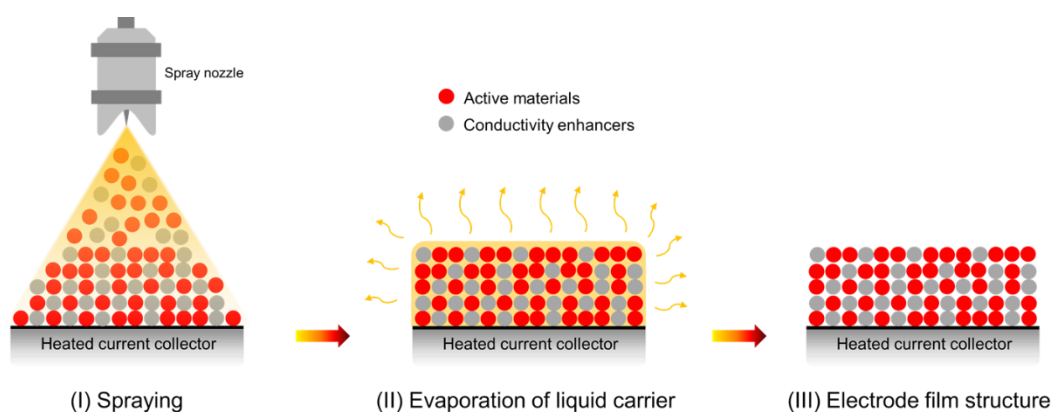


Figure S4. Schematic diagrams describe a mechanism of how the binder-free electrode structure is assembled by the layer-by-layer spray coating process. The effective *in-situ* drying of suspension droplets on the heated current collector could lead to the appropriate inter-connection between electrode constituents even with few binder materials, providing advantageous porosity and tortuosity within overall electrode structures.

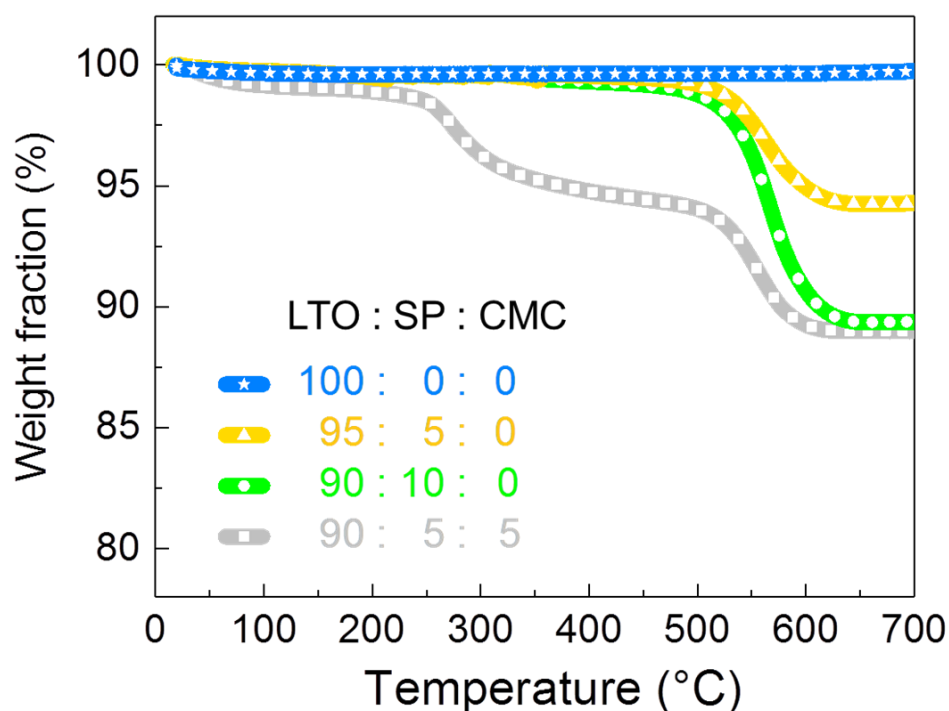


Figure S5. The TGA curves for the spray-coated binder-free LTO electrodes as a function of the SP fraction, ranging from 10 to 0 wt%. To prepare the TGA samples, the electrode layer was carefully separated from the Cu foil. The electrode fragments were then subjected to heating in ambient air, gradually increasing the temperature up to 700 °C. Additionally, the spray-coated electrode formulated with a LTO:SP:CMC mass ratio of 90:5:5 was prepared, which intended to identify the mass change attributed to the SP and CMC fractions. The TGA curve for the 90:5:5 electrode revealed distinct decreases in electrode weights between the temperature ranges of 200 and 500 °C and 500 and 700 °C, which corresponded to the decomposition of 5 wt% CMC and 5 wt% SP, respectively. Based on the TGA data, it was verified that the electrodes with 100:0:0, 95:5:0, and 90:10:0 formulations consist of SP fractions of approximately 0, 5, and 10 wt%, respectively. Furthermore, no CMC binder fraction was included in the electrodes.

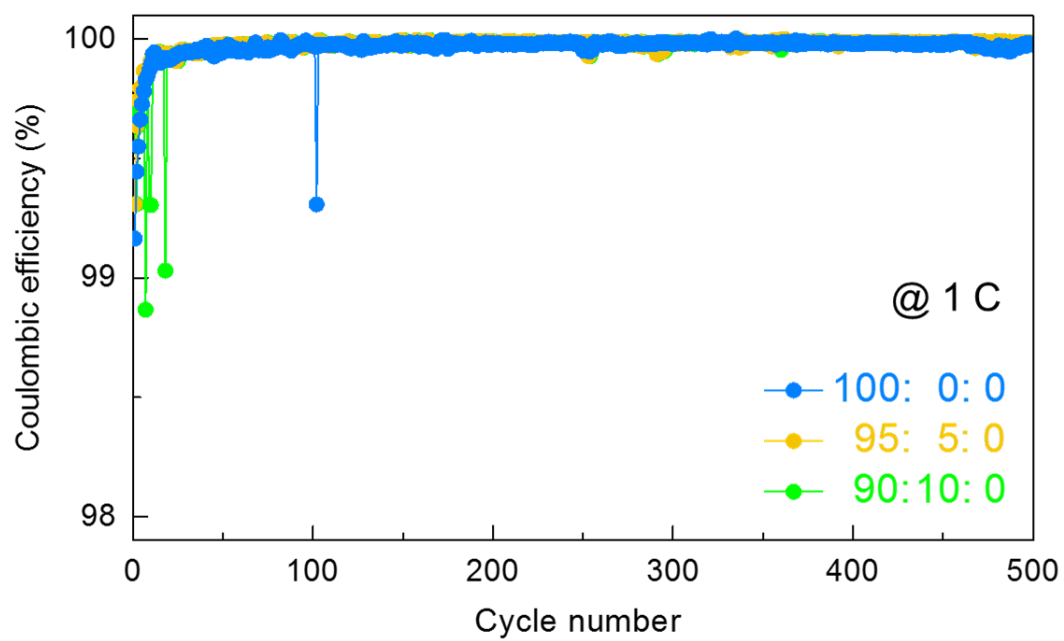


Figure S6. Corresponding coulombic efficiency profiles for the galvanostatic discharge cycles in Figure 5c.

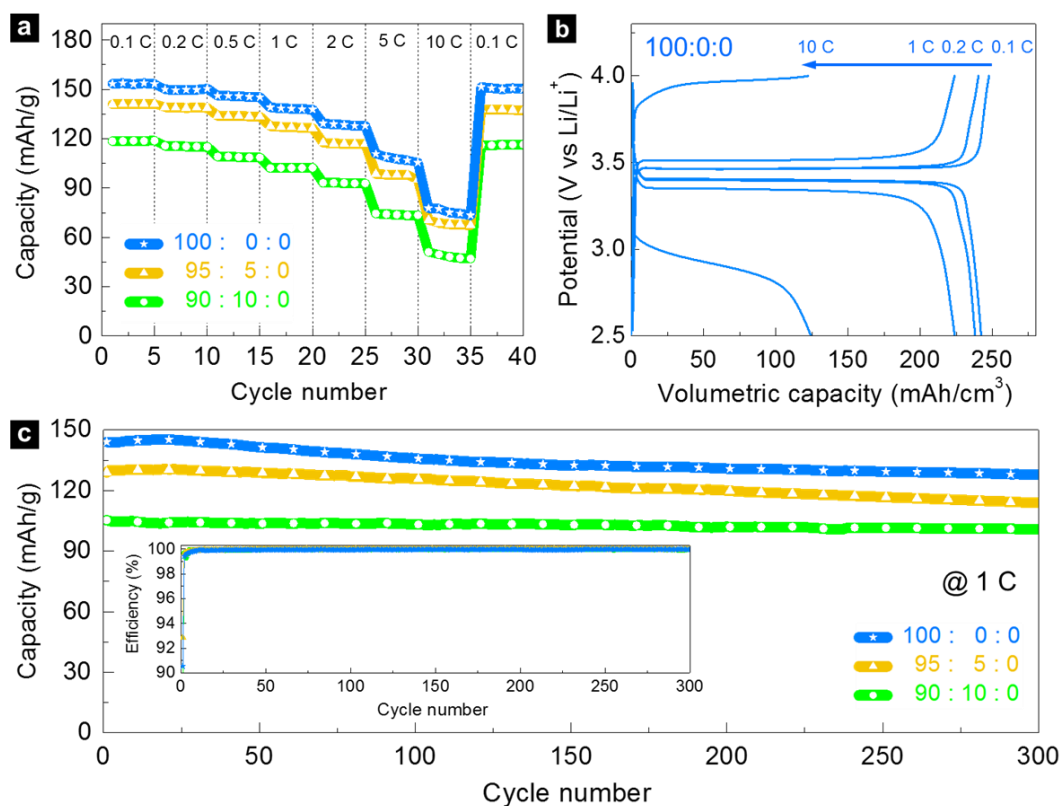


Figure S7. (a) Gravimetric discharge capacity profiles of the spray-coated LFP electrodes as a function of SP and CMC fractions at increasing C-rates in the potential range 2.5 to 4.0 V (vs. Li/Li⁺). (b) Volumetric charge/discharge curves of the spray-coated additive-free LFP electrode (100:0:0 formulation) at 0.1, 0.2, 1 and 10 C in the potential range 2.5 to 4.0 V (vs. Li/Li⁺). (c) Galvanostatic discharge capacity profiles of the spray-coated LFP electrodes at a constant charge/discharge rate of 1 C in the potential range 2.5 to 4.0 V (vs. Li/Li⁺). The inset shows the corresponding coulombic efficiency for the same electrodes.

Table S1. Summary of the spray-coated LFP electrodes as a function of SP and CMC fractions.

Formulation (LFP : SP : CMC)	Thickness (μm)	Mass loading (mg/cm^2)	Discharge capacity (mAh/g)			
			0.1 C	0.2 C	1 C	10 C
90 : 10 : 0	20 ± 2	3.04 ± 0.03	119	116	102	51
95 : 5 : 0	20 ± 2	3.12 ± 0.04	141	139	128	70
100 : 0 : 0	20 ± 2	3.18 ± 0.02	153	150	139	78

Table S2. Comparative performance of LTO/LFP-based LIBs.

Processing ^[a]	Material ^[b]	Formulation ^[c]	Discharge capacity			Reference
			0.1 C	1 C	10 C	
Spray coating	Commercial	100 : 0 : 0	165 mAh/g	138 mAh/g	95 mAh/g	This work
Slurry casting	Carbon-coated	80 : 10 : 10	120 mAh/g	90 mAh/g	-	Ref. [37]
Slurry casting	Ce- or La-doped	80 : 15 : 5	-	119 mAh/g	-	Ref. [38]
Slurry casting	V-doped	80 : 10 : 10	-	170 mAh/g	80 mAh/g	Ref. [39]
Slurry casting	Commercial	75 : 15 : 15	-	145 mAh/g	85 mAh/g	Ref. [40]
Slurry casting	Graphene-doped	80 : 10 : 10	-	130 mAh/g	117 mAh/g	Ref. [41]

^[a] Electrode manufacturing methods.

^[b] Types of active LTO materials.

^[c] Mass ratios of LTO, conductivity enhancers and binders within electrodes.